KSCE Journal of Civil Engineering 30 (2026) 100460

Contents lists available at ScienceDirect

KSCE Journal of Civil Engineering

journal homepage: www.elsevier.com/locate/kscej

Quantifying impacts of precipitation and evapotranspiration on future runoff in the Han River basin using the Budyko framework

Da Hee Hong [a], Jeongwoo Han [b], Hyun-Han Kwon [c], Tae-Woong Kim [d,*]

[a] Department of Civil and Environmental System Engineering, Hanyang University, Ansan 15588, South Korea
[b] Member, Department of Civil and Environmental Engineering, Kunsan National University, Gunsan, Jeonbuk 54150, South Korea
[c] Member, Dept. of Civil and Environmental Engineering, Sejong University, Seoul 05006, South Korea
[d] Member, Dept. of Civil and Environmental Engineering, Hanyang University (ERICA), Ansan 15588, South Korea

ARTICLE INFO

Keywords:
Budyko analysis
Climate change
Runoff
Precipitation
Evapotranspiration
GR4J

ABSTRACT

Changes in hydrometeorological variables due to climate change are expected to affect changes in runoff, posing challenges for water resource management and increasing the risk of economic and environmental hazards. This study simulated future runoff for the Han River basin using the GR4J under different climate change scenarios. The climate elasticity approach, based on the Budyko framework, quantified the contributions of precipitation (P) and potential evapotranspiration (PET) to changes in runoff. Runoff was projected to increase for the near future (NF, 2021–2060) and far future (FF, 2061–2100) compared to the baseline period (BP, 1975–2020). Runoff increased by 22.39 % for NF and 34.72 % for FF under the SSP2–4.5 scenario and by 27.46 % for NF and 48.45 % for FF under the SSP5–8.5 scenario. The aridity index (PET/P) decreased by 0.08–0.09, indicating a shift toward a more humid climate. Because PET and P contributed to changes in runoff by 11 %–24 % and 67 %–84 %, respectively, P was identified as the main cause of the change therein. The findings of this study can be beneficial for water resource management and establishing climate change adaptation measures for the Han River basin.

1. Introduction

Although global warming began when the Industrial Revolution started in the early 1830s, it has accelerated since the 1960s, contributing to the increase in variability of hydrometeorological factors, including temperature, precipitation, and evapotranspiration (Doi & Kim, 2022; IPCC, 2023; Song et al., 2023). The global mean temperature has increased and is expected to increase further for the remaining 21st century under climate change scenarios, such as the Shared Socioeconomic Pathways (SSP) and Representative Concentration Pathway (RCP) scenarios (IPCC, 2023). Furthermore, precipitation characteristics have been altered under climate change across most of the globe, posing greater challenges in water management (IPCC, 2023). Doi and Kim (2022) projected the mean annual temperature and the daily maximum temperatures using the Coupled Model Intercomparison Project Phase 6 (CMIP6) under SSP2–4.5 and SSP5–8.5 scenarios for the period of 2071–2100. They showed that compared to the base period of 1981-2010, the mean annual temperature (the daily maximum temperature) would increase up to 3 °C (10.3 %) and 5 °C (20 %), respectively, under each climate scenario. Song et al. (2023) showed gradual increases in potential evapotranspiration (PET) across the global land areas under the SSP1–2.6, SSP2–4.5, SSP3–7.0, and SSP5–8.5 scenarios. The PET was estimated by the Penman-Monteith method, which used meteorological inputs from 14 different CMIP6 Global Climate Models (GCMs). As representative climatic phenomena under global warming, high-intensity precipitation with a longer intermittent period and an increase in PET have increased the likelihood of extreme floods and drought events (Trenberth, 2005; Nigatu et al., 2021). Trenberth (2005) analyzed the impacts of climate change over various countries and showed elevated risks of floods and droughts during spring and summer, respectively, in mid- and high-latitude regions. Nigatu et al. (2021) demonstrated increases in intensity and frequency of droughts and floods in the Nile River basin of Africa since 1988, using the Water Storage Deficits Index and the Palmer Drought Severity Index. Recent studies suggest that the intensification of hydrological extremes, such as floods and droughts, may persist or even intensify under future climate scenarios (Ekolu et al., 2025; Malede et al., 2025). Ekolu et al. (2025) projected an increasing trend in flood frequency for West Africa due to

* Corresponding author.
E-mail address: twkim72@hanynag.ac.kr (T.-W. Kim).

https://doi.org/10.1016/j.kscej.2025.100460
Received 16 December 2024; Received in revised form 23 July 2025; Accepted 2 November 2025
Available online 10 November 2025

intensified precipitation and rising temperatures, while droughts are also projected to become more severe. In addition, Malede et al. (2025) emphasized that climate change on the global scale has altered the hydrological regime of the Blue Nile Basin, intensifying rainfall and flood risks in humid regions and leading to more frequent, prolonged, and severe droughts in arid regions. These findings imply the likelihood of more severe hydrologic extremes due to a higher variation of runoff and terrestrial water storage under global warming, posing a challenge in water resource management. The monsoonal precipitation for South Korea brings up a dominant seasonal pattern in precipitation in summer, potentially leading to uneven water supply year-round. Therefore, establishing a water resource management plan for sustainable water use and flood mitigation is important for South Korea. However, climate change has perturbed this precipitation pattern, leading to increased variability and unpredictability. In consequence, the pattern of runoff has changed significantly, posing a greater challenge for water resources management. Therefore, understanding changes in runoff and the associated meteorological factors under climate change is beneficial for establishing a reliable water management plan to support sustainable water supply and flood mitigation.

Over the past few decades, the Budyko framework has been widely used to separate factors that affect runoff and to analyze their impact on changes in runoff (Xiong et al., 2020; Krajewski et al., 2021; Ma et al., 2023). Xiong et al. (2020) applied the complementary Budyko (CB), total differential Budyko (TDB), and decomposition Budyko (DB) models for the Heihe River basin in China from 1961 to 2014 to quantify the effects of climate change and land use/cover change on runoff. They showed that land use/cover change contributed to decrease in runoff by 65.20–66.42 %, 65.01–66.57 %, and 64.83–66.85 % when using CB, TDB, and DB, respectively. Krajewski et al. (2021) used the climate elasticity method based on the Budyko framework (hereafter, referred to as CEMBF) to examine the Zagożdżonka River basin in Poland from 1962 to 2015. They showed that climate change reduced annual mean runoff by 60–80 %, while land use changes contributed to the decrease by 20–40 %, highlighting the significant impacts of climate change on the change in runoff volume. Ma et al. (2023) applied the CEMBF to quantify the impacts of climate change and human activities on runoff and sediment discharge for the Taohe River basin in China from 1960 to 2019. They showed that climate change contributed to changes in runoff and sediment discharge by 24.33 % and 2.63 %, respectively, while human activities (e.g., land use changes and water infrastructure construction) contributed to them by 75.67 % and 97.37 %, respectively. However, while most studies used observed data to identify factors that affect changes in runoff, it is difficult to find previous studies that quantified impacts of climate change from the lenses of specific attribute variables, such as precipitation and PET. To gain a deeper understanding of the impacts of climate change on runoff, it is essential to analyze the contributions of future precipitation and PET to change in runoff under different climate change scenarios.

The SSPs are simulated under different climate change scenarios and provide future climate data, such as daily precipitation, maximum and minimum temperatures, relative humidity, and solar radiation. However, since runoff data are not included in the SSP datasets, hydrological models are additionally performed to obtain the future runoff forced by future climate data. Several studies have recently utilized the GR4J (Génie Rural à 4 paramètres Journalier) to simulate runoff in South Korea (Birhanu et al., 2018; Ahn & Kim, 2019; Shin & Jung, 2022). The GR4J is suitable for regions with limited hydrological data since it is a simple conceptual water balance model that requires fewer hydrometeorological variables (Anshuman et al., 2021; Badika et al., 2024). While long-recorded precipitation and temperature data are available for South Korea, streamflow and soil moisture data are limited. Therefore, runoff simulation was done using the GR4J to overcome the data limitation for the study. The GR4J demonstrated better performance in estimating streamflow than other hydrological models (Barbhuiya et al., 2024; Darbandsari & Coulibaly, 2020; Wang et al., 2021). Barbhuiya et al. (2024) compared the GR4J with the Soil and Water Assessment Tool (SWAT) and machine learning models, including Random Forest, Artificial Neural Network (ANN), and Long Short-Term Memory, for streamflow simulation for the northern Himalayan region of India. They showed that the GR4J estimated streamflow accurately, with an average Nash-Sutcliffe Efficiency (NSE) of 0.78. For the Big East River and Black River watersheds in Canada, the GR4J simulated high flows accurately, with an average NSE of 0.82, outperforming the HBV(Hydrologiska Byråns Vattenbalansavdelning) and the HYMOD (Hydrological Model). Also, Wang et al. (2021) showed that the GR4J is applicable to humid regions, including the Daixi, Hengtangcun, and Qiaodongcun catchments in Zhejiang Province, China. With an average NSE of 0.83, the GR4J outperformed Xinanjiang, SimHyd, and ANN models for those regions.

This study aims to analyze the impacts of precipitation and PET on changes in future runoff for sub-basins in the Han River basin of South Korea using the Budyko framework. The future runoff was forecasted by the GR4J using projected precipitation and temperature data from 16 GCMs of CMIP6 under the SSP2–4.5 and SSP5–8.5 scenarios. To analyze the impacts of climatic drivers without accounting for structural differences in hydrological models, a single hydrological model (herein, the GR4J) was consistently applied across all GCM inputs. However, this approach may not address uncertainty from model performance. In addition, anthropogenic factors such as land use changes, urbanization, and dam operations were not considered, as this study focused on the effects of climatic drivers on runoff variability. The Han River basin is already highly urbanized, and future land use changes are unlikely to be significant. Therefore, this study focused on assessing runoff responses to changes in precipitation and potential evapotranspiration without the influence of anthropogenic factors. Previous studies have mainly analyzed the drivers of runoff change based on historical data or quantified impacts of climate change without distinguishing the contributions of precipitation and evapotranspiration. However, this study quantified the influences of precipitation and potential evapotranspiration on runoff under climate change scenarios, extending the applicability of the Budyko framework.

2. Study area and data

The Han River basin has a drainage area of 26,018 km^2 and a channel length of 481.7 km. It includes large metropolitan areas with high populations that require a large amount of water supply in South Korea. Therefore, effective water resource management is critical for that basin. This study obtained inflow data for the five dams within the Han River basin from the Water Management Information System (WAMIS, https://www.wamis.go.kr). As the observation periods differed across the five dams, the period from 2001 to 2020 was used= as a common period to ensure consistent analysis. Although the observation period is limited to 20 years, previous studies have shown that GR4J can produce reliable results using even shorter time series. For example, Munajat (2020) successfully applied GR4J using 10 years of daily runoff data in the Upper Citarum watershed, achieving reasonable model performance. Precipitation, extraterrestrial solar radiation, and the average, maximum, and minimum temperature data at a daily scale for the period of 1975–2020 were collected from 60 weather stations within the basin (Korea Meteorological Administration (KMA); https://www.data.kma.go.kr) (Fig. 1). The meteorological data were spatially interpolated using the Thiessen polygon method to represent meteorological conditions for each sub-basin. Dam inflow data were utilized as reference data to calibrate the GR4J, while temperature and solar radiation data were used to estimate PET. The temperature-based Hargreaves method is effective for regions with limited meteorological data availability (Lujano et al., 2023) as given in Eq. (1).

$$\mathrm{PET} = 0.0023 \times (T_{max} - T_{min})^{0.5}(T_{mean} + 17.8) \times R_a \quad (1)$$

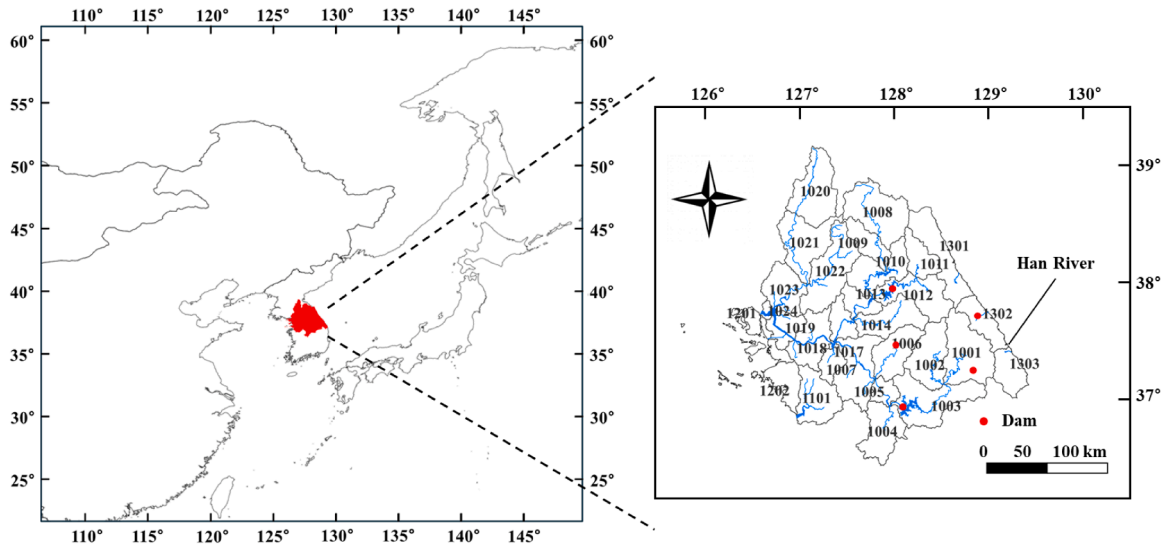

Fig. 1. Location of the Han River basin in South Korea. The numbers in the right figure are the codes of sub-basins.

where T_{max}, T_{min}, and T_{mean} are maximum, minimum, and average temperatures, respectively, in °C. R_a is extraterrestrial radiation, which accounts for theoretical solar energy input. Thus, Eq. (1) represents the amount of water that can be evaporated or transpired in mm/day.

To investigate the impacts of climate change on runoff, the daily precipitation, maximum temperature, and minimum temperature data under the SSP2–4.5 and SSP5–8.5 scenarios were collected for 2021–2100. Table 1 provides basic information on the 16 GCMs used in this study, which exhibit substantial differences in Equilibrium Climate Sensitivity (ECS), leading to projections that may differ by model (IPCC, 2021). ECS refers to the long-term global average of the increase in surface temperature in response to a doubling of atmospheric carbon dioxide relative to pre-industrial levels (Flynn & Mauritsen, 2020). For example, IPSL-CM6A-LR and CanESM5 exhibit high sensitivity, whereas GFDL-ESM4 and MRI-ESM2-0 exhibit relatively low sensitivity to changes in carbon dioxide (Zelinka et al., 2020). It is crucial to use diverse models to assess the uncertainty in projected climate variables used in hydrological modeling. The SSP scenarios describe future socio-economic developments and potential climate-mitigation pathways (Siabi et al., 2023), along with the radiative forcing levels of SSP2-4.5 and SSP5-8.5 that correspond to RCP4.5 and RCP8.5, respectively (O'Neill et al., 2016; Song et al., 2022).

Table 1
GCM climate models used in this study.

No	Model	Institution	Resolution (Lat.× Lon.°)
1	GFDL-ESM4	Geophysical Fluid Dynamics Laboratory (USA)	1.0 × 1.25
2	MRI-ESM2–0	Meteorological Research Institute (Japan)	1.13×1.13
3	CNRM-CM6–1	Centre National de Recherches Meteorologiques (France)	1.4 × 1.4
4	CNRM-ESM2–1		
5	IPSL-CM6A-LR	Institute Pierre-Simon Laplace (France)	2.5 × 1.26
6	MPI-ESM1–2-HR	Max Planck Institute for Meteorology (Germany)	0.94×0.94
7	MPI-ESM1–2-LR		1.88×1.88
8	UKESM1–0-LL	Met Office Hadley Centre (UK)	1.88×1.25
9	ACCESS-CM2	Commonwealth Scientific and Industrial Research Organisation, Australian Research Council Centre of Excellence for Climate System Science (Australia)	1.88×1.25
10	ACCESS-ESM1–5	Commonwealth Scientific and Industrial Research Organisation (Australia)	1.88×1.24
11	CanESM5	Canadian Centre for Climate Modelling and Analysis (Canada)	2.81×2.81
12	EC-Earth3	EC-Earth-Consortium	0.70×0.70
13	MIROC6	Japan Agency for Marine-Earth Science and	1.41×1.41
14	MIROC-ES2L	Technology/Atmosphere and Ocean Research InstituteA/National Institute for Environmental Studies/RIKEN Center for Computational Science (Japan)	2.81×2.81
15	NorESM2-LM	NorESM Climate modeling Consortium consisting of CICERO (Norway)	2.5 × 1.88
16	KACE–1–0-G	National Institute of Meteorological Sciences/Korea Meteorological Administration (Korea)	1.88×1.25

This study used CMIP6 under the SSP2–4.5 and SSP5–8.5 scenarios. SSP2–4.5 represents a middle-of-the-road scenario in which the world population is projected to grow at a moderate rate, and the income levels among countries converge slowly. On the other hand, SSP5–8.5 represents a world with strong economic growth driven by high greenhouse gas emissions (Gidden et al., 2019; Vo et al., 2024).

This study used GCM data that underwent bias correction and statistical downscaling, following Hur et al. (2024), to produce a product with a 1 km spatial resolution on a daily temporal scale. ERA5 reanalysis data with a spatial resolution of 25 km was used as input to the Parameter-elevation Regressions on Independent Slopes Model (PRISM; Daly et al., 1994), which can account for the topographic effects of complex terrain in doing spatial interpolation and, in turn, performs bias correction using in-situ observations to construct a high-resolution climatic input field over the Korean Peninsula.

As a nonparametric bias correction method, simple quantile mapping (SQM) was applied to match quantiles between the observations and GCM-simulated daily values for the historical period (1981–2010). Then, the mapping relationships were applied to future climate projections (2011–2100) to statistically correct biases of the downscaled datasets. This procedure was implemented using the SQMGrid package (Cho et al., 2018). For precipitation, a dry-day correction was also applied (Themeßl et al., 2011).

Detailed discussions of the SQM method, including the dry-day correction are found in Hur et al. (2024) and Cho et al. (2018).

3. Methodology

3.1. The GR4J and parameter estimation

The GR4J was employed to simulate future runoff under the SSP2–4.5 and SSP5–8.5 scenarios, and the simulations were implemented using the airGR R package. The GR4J model, as a lumped rainfall-runoff model based on a conceptual two-bucket model, has four parameters and performs channel routing using a unit hydrograph (Noh et al., 2024). The conceptual structure of the GR4J model is shown in Fig. 2, in which P represents precipitation, PET represents potential evapotranspiration, P_n represents the net precipitation, PET_n represents net PET, P_s represents the precipitation that infiltrates into the production store, $P_n - P_s$ represents the precipitation that contributes to runoff, P_r represents the flow component that reaches the routing store, PET_s represents evaporation from the production store, S represents the storage in the production store, $Perc$ represents percolated water, R represents the storage in the routing store, and Q represents total runoff.

The GR4J partitions the P and PET into P_n and PET_n by subtracting PET from P as

$$If\ P \geq PET,\ then\ P_n = P - PET\ and\ PET_n = 0$$

$$otherwise\ P_n = 0\ and\ PET_n = PET - P \quad (2)$$

In sequence, P_n and PET_n drain to the production store. When P_n is not zero, P_s of P_n, which represents the infiltrated P, fills the production store. The flow component P_r, which consists of percolated flow $Perc$ from the production store and the flow component $P_n - P_s$, is obtained by summing these two components as Eq (3) (Séne et al., 2024).

$$P_r = Perc + (P_n - P_s) \quad (3)$$

In the model, 90 % of P_r is routed by a unit hydrograph UH1 and travels through the additional routing process in the routing store. The remaining 10 % of P_r is routed by a second unit hydrograph UH2 (Perrin et al., 2003). The resulting runoff is estimated by combining the outputs from these two routed flows.

The four parameters of the GR4J represent the maximum storage capacity of the production storeX_1 (mm), the groundwater exchange

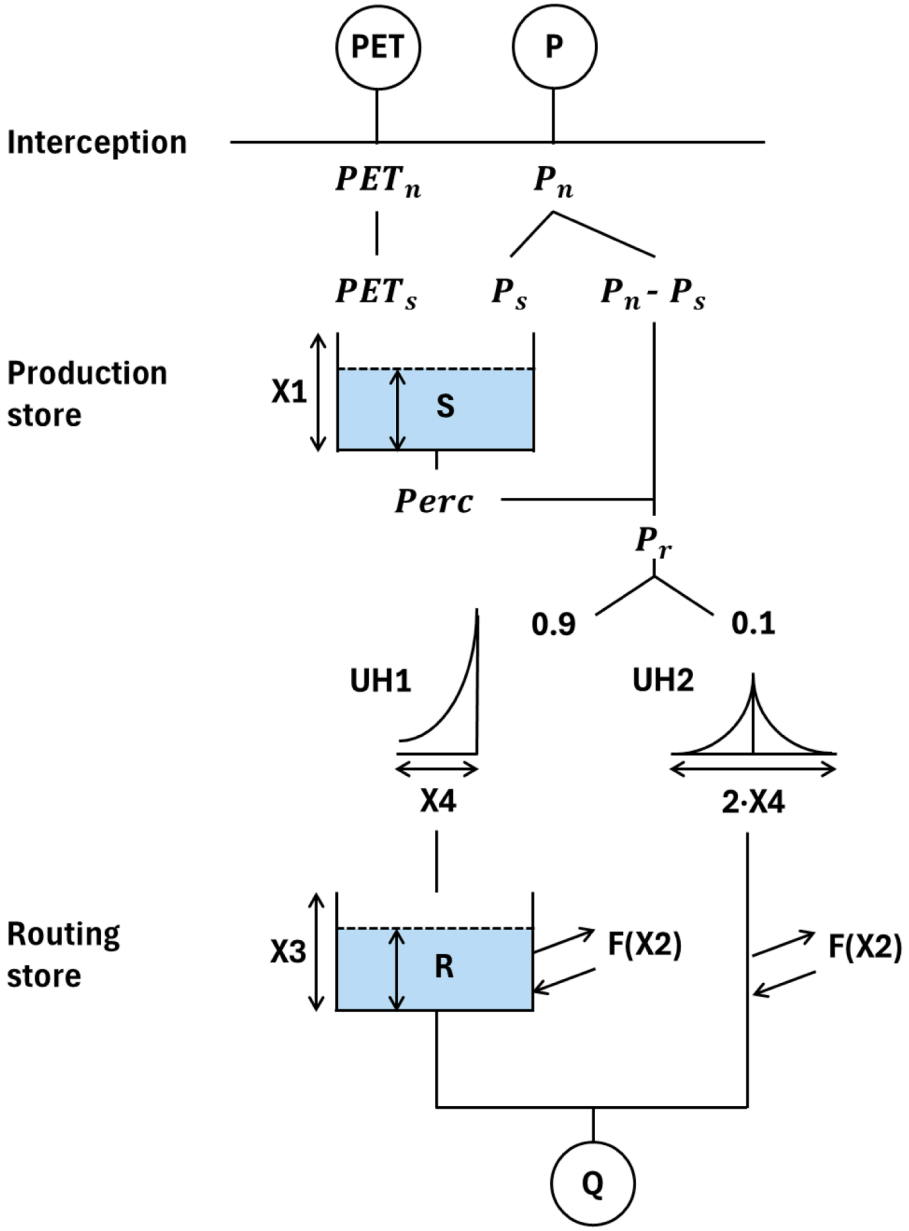

Fig. 2. Diagram of the GR4J rainfall-runoff model.

coefficient X_2 (mm), the maximum storage capacity of the routing store X_3 (mm), and the time to peak for the unit hydrograph X_4 (days) (Meresa et al., 2022). Table 2 lists definitions of the parameters of the GR4J and their ranges (Demirel et al., 2013).

Parameters of the GR4J were calibrated using Michel's optimization method in the R package. This method typically calibrates parameters based on the NSE coefficient as a loss function. For this study, parameters were calibrated by an iterative optimization scheme with 100 iterations. Furthermore, NSE and Kling-Gupta Efficiency (KGE) were used as error metrics to quantify the model accuracy for the validation period. The NSE tends to overestimate errors in high flows due its squaring terms; in contrast, the KGE accounts for correlation, bias, and varianace, which enables a more comprehensive assessment across both high and low flows (Santos et al., 2018). The NSE and KGE are widely used error metrics for validation of hydrological models and are expressed as (Gupta et al., 2009; Knoben et al., 2019)

$$NSE = 1 - \frac{\sum_{t=1}^{T}(Q_{obs}(t) - Q_{sim}(t))^2}{\sum_{t=1}^{T}(Q_{obs}(t) - \overline{Q_{obs}})^2} \tag{4}$$

$$KGE = 1 - \sqrt{(r-1)^2 + (\beta-1)^2 + (\gamma-1)^2} \tag{5}$$

where $Q_{obs}(t)$ and $Q_{sim}(t)$ denote observed and simulated streamflow at day t, respectively. $\overline{Q_{obs}}$ is the average value of observed streamflow, r represents the Pearson's correlation coefficient, β is the ratio of the mean of estimates to that of observations, and γ denotes the ratio of the standard deviation of estimates to that of observations.

When the values of NSE and KGE are 1, the model performs best, indicating that the simulated runoff is perfectly consistent with the observed runoff (Akhtar et al., 2022; Gu et al., 2023).

3.2. Spatial proximity model

This study employed the spatial proximity model to simulate past and future runoff in ungauged basins. The spatial proximity approach transfers parameters or streamflow from neighboring catchments to an ungauged catchment under the assumption that closely located catchments have a similar hydrogeological regime since climate and catchment characteristics are not likely to vary abruptly (Oudin et al., 2008). The runoff for ungauged basins can be obtained using either the parameter averaging method or the runoff averaging method as Eqs. (6) and (7), respectively.

$$\widehat{Q}(j) = \widehat{Q}\left(j, \frac{\sum_{i=1}^{n} X_i}{n}\right) \tag{6}$$

$$\widehat{Q}(j) = \frac{1}{n}\sum_{i=1}^{n}\widehat{Q}(j, X_i) \tag{7}$$

where $\widehat{Q}(j)$ is streamflow for day j, n is the number of donor (gauged) catchments, and X_i is the vector of model parameter values for donor catchment i. This study applied the parameter averaging method that has shown relatively higher predictive performance (Parajka et al., 2005; Oudin et al., 2008).

Table 2
Parameters of the GR4J and their ranges.

Parameter	Description	Range
X_1	Maximum capacity of the Production Store (mm)	10 ~ 2000
X_2	Groundwater exchange coefficient (mm)	−8 ~ 6
X_3	Maximum capacity of routing store (mm)	10 ~ 500
X_4	Time peak ordinate of hydrograph unit UH1 (day)	0 ~ 4

3.3. Budyko framework

Based on the Budyko hypothesis, the Budyko framework partitions precipitation into evapotranspiration and runoff (Collignan et al., 2023). The Budyko hypothesis establishes an interaction between the water balance and energy balance to estimate runoff and evapotranspiration from precipitation: the energy balance estimates evapotranspiration by energy availability, such as solar radiation, such that evapotranspiration varies with changes in energy supply. In sequence, runoff is estimated based on the water balance by subtracting evapotranspiration from precipitation. Budyko (1974) proposed an empirical Budyko equation, Eq. (8), which can explain both water and energy balance based on the Budyko hypothesis.

$$\frac{AET}{P} = F(\varphi) = \left[\frac{PET}{P}\tanh\frac{P}{PET}\left(1 - e^{-\frac{PET}{P}}\right)\right]^{0.5} \tag{8}$$

where $\varphi\left(=\frac{PET}{P}\right)$ is the aridity index, expressed as the ratio of PET to P.

The Budyko equation is based on the theory of water and energy limits (Fig. 3); in the humid state ($\varphi < 1$), evapotranspiration is limited by total available energy. In comparison, in the arid state ($\varphi > 1$), water availability limits the evapotranspiration process (Sinha et al., 2018). If hydroclimatic changes occur, the state of the watershed changes from A to B. In the case involving only the climate change, the evaporation index ($\frac{AET}{P}$) changes according to the change of the aridity index, and the state of the watershed moves from A to a different point B on the same Budyko curve (Kim et al., 2021).

In this study, Eq. (9) was used as the Budyko equation since, unlike the traditional Budyko equation, it explains the hydrological cycle of catchments by effectively capturing the interactions between water and energy in humid and arid regions (Zhang et al., 2001).

$$\frac{AET}{P} = \frac{1 + \omega\left(\frac{PET}{P}\right)}{1 + \omega\left(\frac{PET}{P}\right) + \left(\frac{PET}{P}\right)^{-1}} \tag{9}$$

where ω is an empirical coefficient to represent plant-available water in soil

3.4. Climate elasticity method

Schaake (1990) developed the climate elasticity coefficient based on the Budyko curve to measure the sensitivity of runoff to the variation of climate variables. The climate elasticity coefficient was defined as the ratio of the change rate in runoff to that in a climate factor (Zheng et al., 2021).

$$\varepsilon_X = \lim_{\Delta X/X \to 0}\left(\frac{\Delta Q/Q}{\Delta X/X}\right) = \frac{\frac{\partial Q}{Q}}{\frac{\partial X}{X}} \tag{10}$$

where X represents the influencing factors of runoff. In this study, P and PET are the influencing factors. Thus, the elasticity coefficient of the runoff (Q), which is affected by P and PET, can be denoted as ε_P and ε_{PET}, respectively (Krajewski et al., 2021).

$$f(\varphi) = \frac{1 + \omega(\varphi)}{1 + \omega(\varphi) + (\varphi)^{-1}} \tag{11}$$

$$f'(\varphi) = \frac{2\omega(\varphi) + 1}{(\omega(\varphi)^2 + (\varphi) + 1)^2} \tag{12}$$

$$\varepsilon_P = \frac{\frac{\partial Q}{Q}}{\frac{\partial P}{P}} = 1 + \frac{\varphi f'(\varphi)}{1 - f(\varphi)} \tag{13}$$

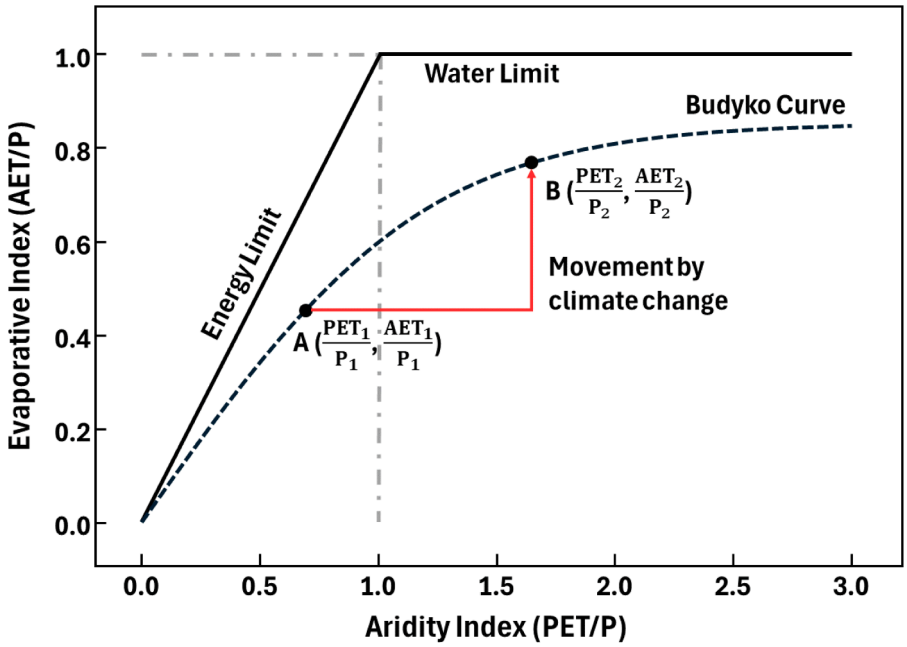

Fig. 3. Variation on the Budyko curve due to climate change.

$$\varepsilon_{PET} = 1 - \varepsilon_P \tag{14}$$

Once ε_P and ε_{PET} are obtained, the contribution of climate change to the change in runoff is expressed as (Chen et al., 2021)

$$\Delta Q_C = \Delta Q_P + \Delta Q_{PET} = \left(\varepsilon_P \frac{\Delta P}{\overline{P}} + \varepsilon_{PET} \frac{\Delta PET}{\overline{PET}}\right) \times \overline{Q} \tag{15}$$

where ΔQ_C, ΔQ_P, and ΔQ_{PET} represent changes in runoff due to changes in climate change, P, and PET, respectively. $\overline{P}$, $\overline{PET}$, and $\overline{Q}$ denote the mean of annual P, PET, and runoff, respectively. The total change in runoff (ΔQ_T) can be expressed as the sum of changes in runoff due to climate change (ΔQ_C) and the change in runoff due to other activities (ΔQ_O):

$$\Delta Q_T = \Delta Q_C + \Delta Q_O = \Delta Q_P + \Delta Q_{PET} + \Delta Q_O \tag{16}$$

Furthermore, the relative contributions of P and PET to a change in runoff are calculated as (Swain et al., 2023)

$$\lambda_P = \frac{\Delta Q_P}{\Delta Q_T} \times 100 \tag{17}$$

$$\lambda_{PET} = \frac{\Delta Q_{PET}}{\Delta Q_T} \times 100 \tag{18}$$

where λ_P and λ_{PET} represent the contributions of P and PET, respectively, to a change in runoff.

The climate elasticity coefficients (ε), as defined in Eqs. (13) and (14), represent the sensitivity of runoff to a change in P or PET. In contrast, the contribution ratios (λ), which are calculated using Eqs. (17) and (18), quantify the actual proportion of runoff change attributed to each climatic factor.

4. Results and discussion

4.1. Future runoff simulation and projection

The future runoff from 2021–2100 for each sub-basin was simulated using the GR4J under the SSP2–4.5 and SSP5–8.5 scenarios. Parameters of the GR4J were calibrated within the parameter ranges listed in Table 2 using runoff, P, PET, and temperature data from 2001 to 2016. The evaluation of model performance using the NSE showed its values ranging from 0.48 to 0.90 for the five dams. Except for one watershed (#1001, the Namhan River Upstream watershed), where the NSE value was less than 0.5, the other dams showed satisfactory performance, based on Table 3. The site (#1001) with the lowest NSE was excluded from the calibrated models belonging to gauged basins. Since it was treated as ungauged, runoff at this site was simulated using the Spatial Proximity Model with GR4J parameters from neighboring gauged basins. Using the estimated parameters for inflows to the four dams with acceptable model accuracy, their inflows were validated for the period of 2017 to 2020 and showed satisfactory NSE and KGE, ranging from 0.63 to 0.83 and 0.73 to 0.81, respectively. The calibrated parameters of the GR4J for the four dams are listed in Table 4, and the NSE and KGE values for the calibration and validation periods are summarized in Table 5.

Fig. 4 shows the estimated daily runoff from the GR4J (orange lines) and the observed runoff (black lines) during the validation period of 2017 to 2020 for the Soyang River watershed (#1012). The estimated runoff adequately mimicked temporal trends and captured peak locations, especially for high-flow regimes in each year, while slight over- and under-estimations were observed for some peak flow events. For the validation period at this sample location, the model yielded NSE of 0.83 and KGE of 0.81. However, the model tended to underestimate runoff in low-flow seasons.

For further model performance analysis, high- and low-flow conditions were defined as runoff exceeding the 90th percentile and less than the 10th percentile, respectively. The model performances for the high- and low-flow for the four dams are listed in Table 5. For the high-flow condition of Soyang River watershed (#1012), the model showed NSE of 0.73 and KGE of 0.75, indicating accurate estimations for high-extreme events (Table 5). In contrast, the model showed degraded

Table 3
Accuracy level of NSE and KGE (Nash & Sutcliffe, 1970; Moriasi et al., 2007).

Performance level	NSE	KGE
Very good	0.75~1.00	0.90~1.00
Good	0.65~0.75	0.75~0.90
Satisfactory	0.5~0.65	0.5~0.75
Unsatisfactory	< 0.5	< 0.5

Table 4
Calibrated parameters of the GR4J.

Watershed Code	X_1	X_2	X_3	X_4
1003	117.413	2.221	86.882	1.249
1006	36.909	1.419	174.094	1.085
1012	10.961	−1.570	157.456	1.143
1302	59.183	1.010	154.821	1.038

Table 5
Accuracy of the GR4J for the calibration and validation periods.

Watershed Code	Calibration NSE	Validation (All-flow)		Validation (High-flow)		Validation (Low-flow)	
		NSE	KGE	NSE	KGE	NSE	KGE
1003	0.83	0.63	0.76	0.27	0.61	−0.53	−2.61
1006	0.74	0.66	0.77	0.45	0.63	−5.12	−56.50
1012	0.90	0.83	0.81	0.73	0.75	−0.51	−3.83
1302	0.85	0.81	0.73	0.75	0.67	−0.74	−18.64

performance (i.e., negative NSE and KGE) for the low-flow conditions for the four dams (Table 5). This degrading accuracy for the low-flow condition is partially attributed to the simplified hydrological process of the GR4J that cannot address the implications of baseflow. However, since this study focused on amounts of runoff at an annual scale rather than its daily dynamics, the model's poor performance for low-flow conditions was not expected to affect the overall findings. Table 6 shows the relative errors between observed and simulated runoff on an annual scale. While relative errors ranged from –20.38 % to 6.14 % during 2017−2020, they were within ±10 % for the period of 2017−2019, indicating that the model reasonably simulates annual runoff except for the year 2020. The largest error in 2020 (–20.38 %) was attributed to the unusually high runoff in that year, which led to significant underestimation. Therefore, the GR4J is applicable to fulfill the objectives of this study.

Additionally, runoff values for 1975−2000 and 2021−2100 were hindcasted and forecasted, respectively, using the calibrated parameters during the observation period. However, as the model performance was unsatisfactory in watershed #1001(the Namhan River Upstream watershed), this basin, along with the 25 sub-basins without dams, was treated as an ungauged basin. To simulate past and future runoff for ungauged basins, the arithmetic mean of the parameters from the four dams was used following the parameter averaging method of the spatial proximity model. Runoff was simulated on a daily scale and aggregated to an annual scale to apply the Budyko equation. Fig. 5 shows the changes in future annual runoff for the Soyang River watershed (#1012) simulated using the GR4J. While the future runoff simulated by different GCMs under the SSP2–4.5 and SSP5–8.5 scenarios showed variability, the average runoff is projected to increase (Fig. 5). Furthermore, the pink-shaded area is narrower under the SSP5–8.5 scenario than under the SSP2–4.5 scenario, indicating a reduced uncertainty.

For this study, the observation period (1975–2020) was set as the baseline period (BP), and the future period was divided into the near

Table 6
Observed and simulated annual runoff and their relative errors for the Soyang River watershed (#1012).

Year	Observed Runoff (mm)	Simulated Runoff (mm)	Relative error (%)
2017	730.93	674.94	−7.66
2018	781.20	829.18	6.14
2019	424.88	414.25	−2.50
2020	1252.43	997.17	−20.38

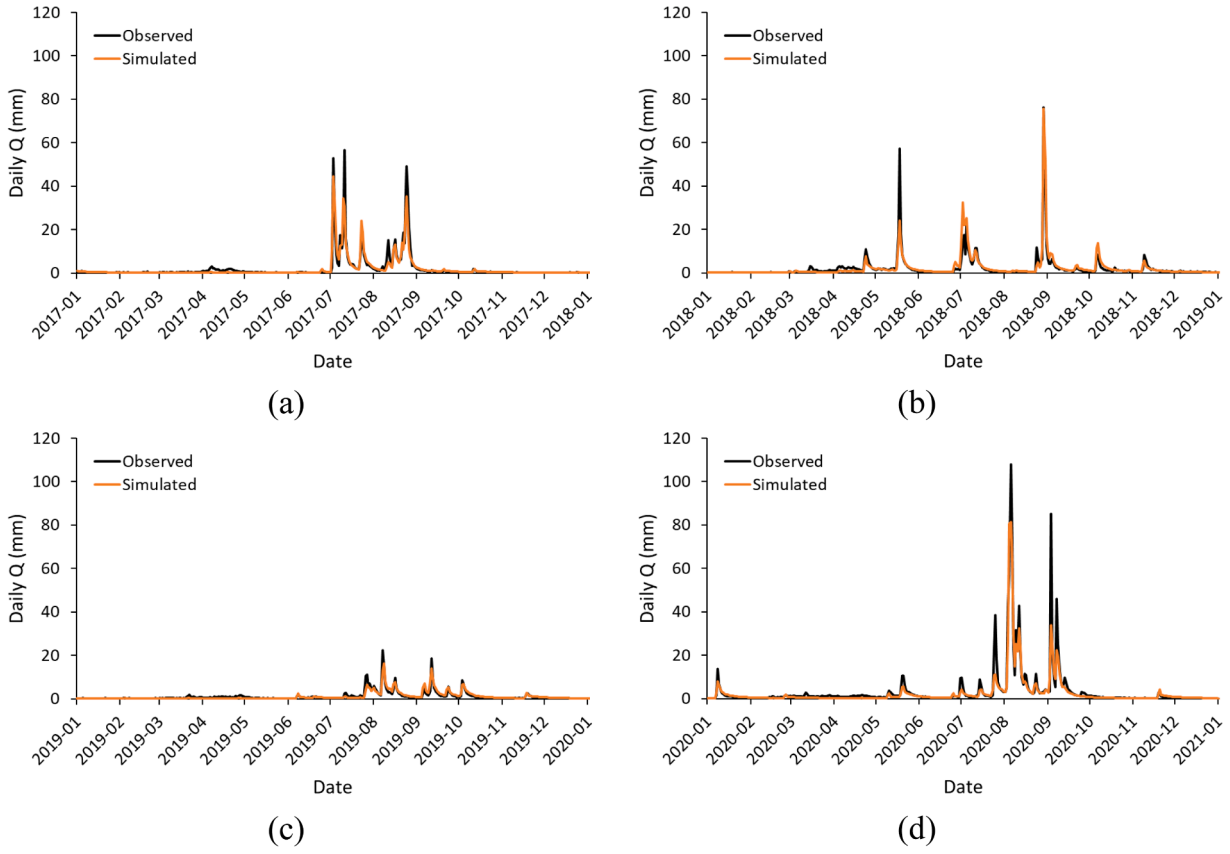

Fig. 4. Observed (black solid lines) and simulated (orange solid lines) daily runoff for the Soyang River watershed (#1012) for years (a) 2017, (b) 2018, (c) 2019, and (d) 2020.

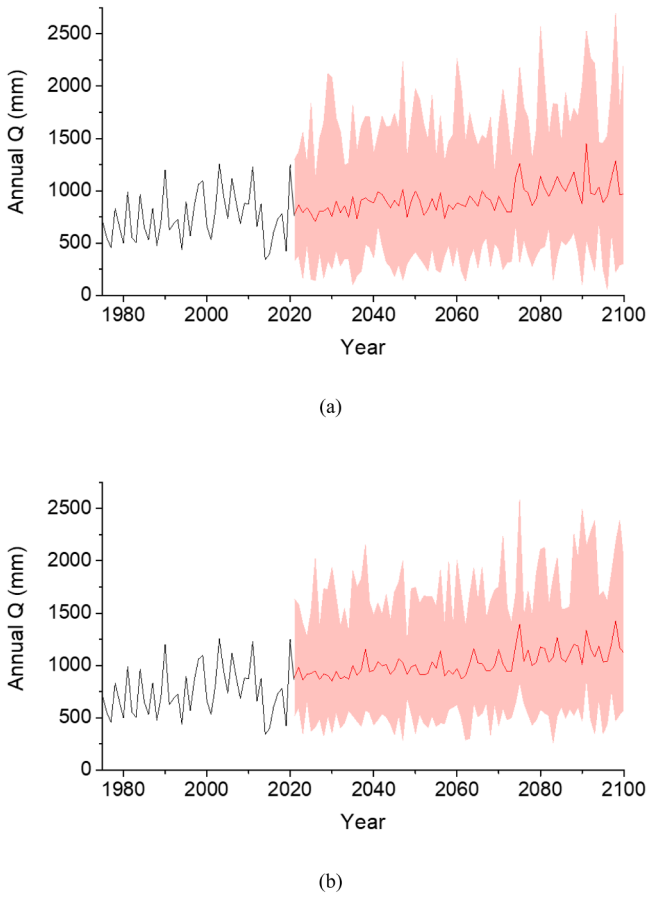

Fig. 5. Changes in the annual runoff for the Soyang River Watershed (#1012) (a) under the SSP2–4.5 scenario and (b) under the SSP5–8.5 scenario. The black line represents the annual runoff during the observation period (1975–2020), while the red line indicates the ensemble average of annual precipitation from 16 GCMs for the future period (2021–2100). The pink-shaded area represents the uncertainty from the 16 GCMs.

future (NF: 2021–2060) and the far future (FF: 2061–2100). Fig. 6 shows box plots that summarize the changes in simulated runoff, P, and PET for 30 sub-basins in the Han River basin under the SSP2–4.5 and SSP5–8.5 scenarios.

Runoff, P, and PET increased for both NF and FF periods compared to the BP, with a greater increase observed for the FF period than the NF period. For the NF and FF periods under the SSP2–4.5 scenario, the average annual runoff increased by 22.39 % and 34.72 %, respectively, compared to the BP, while under the SSP5–8.5 scenario, its increase was 27.46 % and 48.45 %, respectively. The increase in the magnitude of runoff was greater under the SSP5–8.5 than the SSP2–4.5 scenario. Similar trends were observed for changes in P and PET (Fig. 6). For the NF and FF periods under the SSP2–4.5 scenario, the average annual P increased by 14.98 % and 23.85 %, respectively, and the average annual PET increased by 6.88 % and 11.07 %. Under the SSP5–8.5 scenario, the average annual P increased by 18.37 % and 32.95 % for the NF and FF periods, respectively, while the average annual PET increased by 7.68 % and 16.35 %.

4.2. Changes in aridity index

The aridity index (PET/P) can be calculated using P and PET. Fig. 7 presents the aridity index of all basins during the BP in the Budyko space and showed values less than 1.0 for each. This indicates that the Han River basin experienced a humid climate and was under energy-limited conditions. Among the 30 sub-basins, the Namhan River Upstream watershed (#1001: see Fig. 1) had the smallest PET/P value of 0.55, indicating a relatively humid climate. In contrast, the Dalcheon watershed (#1004: see Fig. 1), with the largest PET/P value of 0.87, exhibited a relatively arid climate. During the BP, the Namhan River Upstream watershed (#1001) experienced an average annual P of 1593.55 mm and an average annual PET of 869.86 mm. On the other hand, the Dalcheon watershed (#1005) had an average annual P of 1240.04 mm and an average annual PET of 1079.75 mm. Thus, the Dalcheon watershed had a lower P and a higher PET than the Namhan River Upstream watershed (#1001): a two-tailed *t*-test showed a significant difference in mean annual P between the two basins ($p < 0.001$). In addition, a two-tailed *t*-test of the mean annual PET of the two basins showed a significant difference ($p < 0.001$). Therefore, while the Namhan River Upstream watershed (#1001) with the lowest PET/P value is likely to have a more humid climate, the Dalcheon watershed (#1004) is comparably arid with the highest PET/P among the sub-basins. The PET/P for future periods was calculated and is summarized in Fig. 8 to examine possible future changes in hydroclimatic conditions.

Under the SSP2–4.5 and SSP5–8.5 scenarios, PET/P was expected to decrease. The mean PET/P during BP was 0.77, while that for the NF and FF periods under the SSP2–4.5 scenario were 0.72 and 0.69, respectively. The decrease in PET/P for the future period would be attributed to a greater increase in P than in PET. The substantial increase in annual P is expected to lead to an increase in annual streamflow, as we confirmed in Section 4.1. Thus, as higher-intensity-rainfall is expected in the future, the likelihood of higher-risk-flooding might increase. A one-way analysis of variance was conducted to test whether the mean values of PET/P for the BP, NF, and FF periods differ significantly. The result (F-value of 90.61, $p < 0.001$) indicates that changes in PET/P over the three periods are significant and not by chance. In addition, under the SSP5–8.5 scenario, the mean values of PET/P for the NF and FF periods were 0.71 and 0.68, respectively, with significant differences compared to BP (F-value of 147.80, $p < 0.001$). Under the SSP5–8.5 scenario, the F-value was higher than that under the SSP2–4.5 scenario, indicating more pronounced differences in mean values across periods. These results indicate that the mean PET/P differs significantly across periods, suggesting that the future climate will become more humid as PET/P decreases. As a result, the long-term water balance shifts to the left along the Budyko curve, approaching the energy limit, such that runoff is affected more significantly by P than PET.

4.3. Relative contribution of climate change to runoff variability

In this study, the impacts of P and PET on changes in runoff for 30 sub-basins were quantified using the climate elasticity method based on the Budyko framework. The mean elasticity coefficients of precipitation (ε_P) for the NF and FF periods under the SSP2–4.5 scenario were 1.82 and 1.81, respectively, and those under the SSP5–8.5 scenario were 1.81 and 1.79. The mean elasticity coefficients of PET (ε_{PET}) for the NF and FF under the SSP2–4.5 were −0.82 and −0.81, respectively, while those under SSP5–8.5 scenarios were −0.81 and −0.79. The positive ε_P indicates that P increased runoff, while the negative ε_{PET} implies that it decreased runoff.

Xing et al. (2018) remarked that a large absolute value of the climate elasticity coefficient indicates that runoff is highly sensitive to climatic factors. We showed greater absolute values of the mean ε_P than those of ε_{PET} ($|\varepsilon_{PET}|$), confirming P as a more dominant factor in chagning runoff than PET. Thus, we re-confirm that P is the dominant climatic driver of runoff variability under future climate scenarios. Table 7 presents the climate elasticity coefficients for the Namhan River Upstream watershed (#1001), which has the smallest PET/P value, and the Dalcheon watershed (#1004), which has the largest PET/P value. During the NF period under the SSP2–4.5 scenario, the mean ε_P from the 16 GCMs for the Namhan River Upstream watershed (#1001) was 1.60, which was lower than the average across all watersheds. On the other hand, the

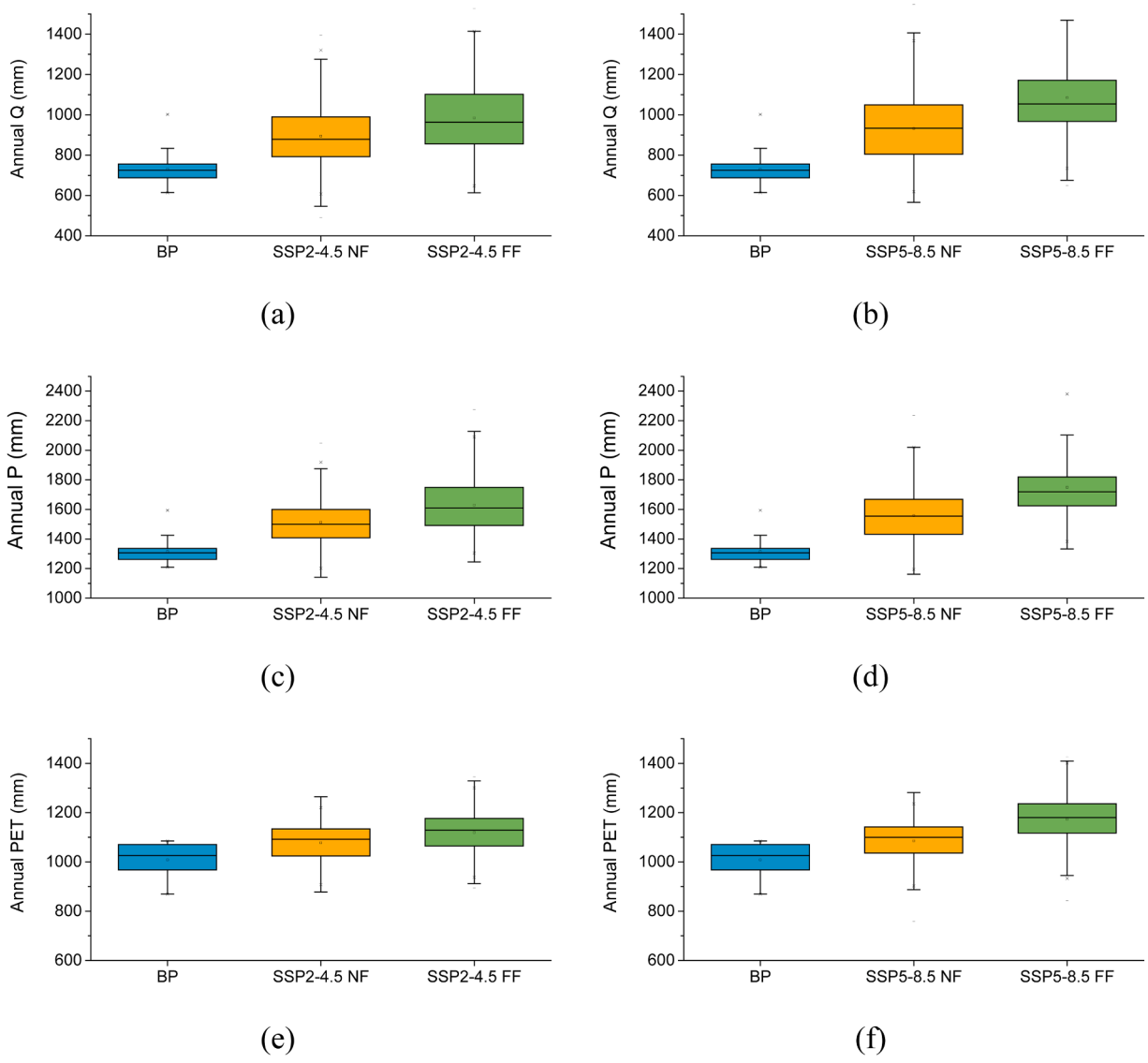

Fig. 6. (a) Comparing the annual runoff of the baseline period with that for the near future and far future under the SSP2–4.5 scenario, (b) the same as (a) but for the future annual runoff under the SSP5–8.5 scenario, (c) the same as (a) but for P, (d) the same as (c) but for the SSP5–8.5 scenario, (e) the same as (a) but for PET, (f) the same as (e) but for the SSP5–8.5 scenario.

mean ε_P for the Dalcheon watershed (#1004) was 1.92, which was higher than the overall average. This indicates that runoff in the Dalcheon watershed (#1004) is relatively more sensitive to P, whereas runoff in the Namhan River Upstream watershed (#1001) is less sensitive to P. The relatively low mean ε_P for the Namhan River Upstream watershed (#1001) can be attributed to its climatic characteristics. This watershed has a low PET/P, indicating a humid climate in which P generally exceeds PET. According to Sankarasubramanian et al. (2001), lower climate elasticity values were observed in humid regions. Therefore, the Namhan River Upstream watershed (#1001), representing a humid climate, showed lower ε_P than the Dalcheon watershed (#1004), which is characterized by relatively drier conditions and lower runoff. During the same period, the mean of ε_{PET} for the Namhan River Upstream watershed (#1001) and the Dalcheon watershed (#1004) were −0.60 and −0.92, respectively, indicating the Dalcheon watershed (#1004) had a larger absolute value. Since the sum of ε_P and ε_{PET} is always equal to 1, a higher value of ε_P corresponds to a higher absolute value of ε_{PET}. This demonstrates that the runoff for the Dalcheon watershed (#1004) was relatively more sensitive to PET, while the runoff for the Namhan River Upstream watershed (#1001) was less sensitive to PET. For the FF period under the SSP2–4.5 scenario, the absolute values of the mean climate elasticity coefficients for the Namhan River Upstream watershed (#1001) and the Dalcheon watershed (#1004) decreased compared to the NF period, indicating that runoff in both watersheds would become less sensitive to P and PET for the FF period than the NF period. Similarly, under the SSP5–8.5 scenario for both the NF and FF periods, the absolute values of the mean climate elasticity coefficients were larger for the Dalcheon watershed (#1004) than for the Namhan River Upstream watershed (#1001). Also, the runoff in the Dalcheon watershed (#1004) was less sensitive to P and PET for the FF period than the NF period.

Fig. 9 illustrates the contributions of P and PET to runoff changes for the NF and FF periods under the SSP2–4.5 and SSP5–8.5 scenarios. P was the primary factor that affected changes in runoff for most GCMs and basins. The λ_P were between 67 % and 84 % for both scenarios, indicating its dominant influence. The median λ_P for the NF and FF under the SSP2–4.5 scenario were 76.94 % and 77.60 %, respectively, and those under the SSP5–8.5 scenario were 77.82 % and 78.21 %. In addition, there was reduced variability for the FF compared with the NF under both scenarios. The median λ_{PET} for the NF and FF under the SSP2–4.5

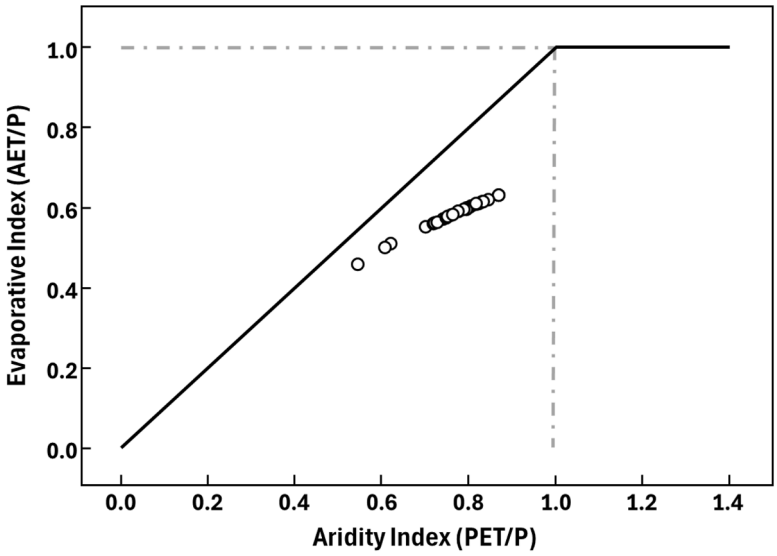

Fig. 7. Hydroclimatic conditions of 30 sub-basins during the base period in the Budyko space. The point represents the hydrological condition of the watershed.

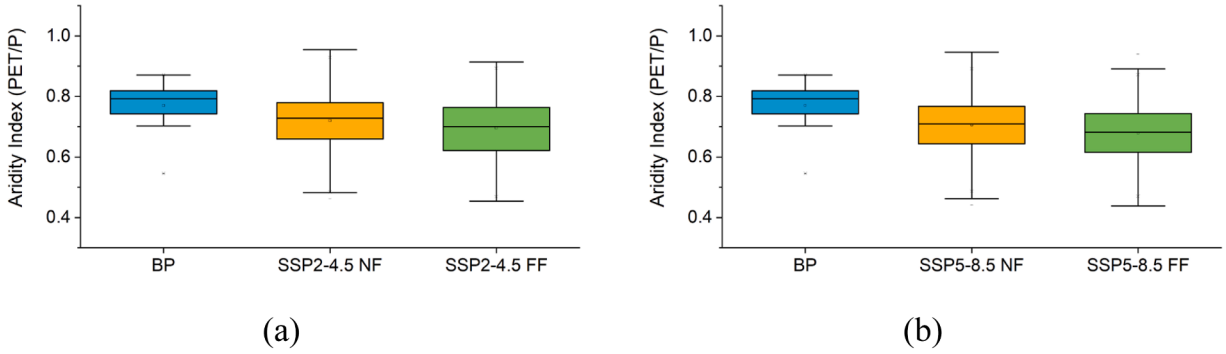

Fig. 8. Boxplot of the aridity index (PET/P) for the base period and the near and far futures (a) under the SSP2–4.5 scenario and (b) under the SSP5–8.5 scenario.

Table 7
Climate elasticity coefficients for the Namhan River Upstream watershed (#1001) and Dalcheon watershed (#1004).

Scenarios	Period	#1001		#1004	
		ε_P	ε_{PET}	ε_P	ε_{PET}
SSP2–4.5	NF	1.60	−0.60	1.92	−0.92
	FF	1.59	−0.59	1.90	−0.90
SSP5–8.5	NF	1.59	−0.59	1.91	−0.91
	FF	1.59	−0.59	1.89	−0.89

scenario was 15.73 % and 17.43 %, respectively, and that under the SSP5–8.5 scenario were 14.78 % and 17.61 %. A slight increase in λ_{PE} for the FF, compared with the NF, was observed under both scenarios. A reduced variability for the FF under the SSP5–8.5 scenario was also observed. Since the elasticity coefficients of P and PET would not change significantly between the NF and FF periods under either scenario, the level of their contribution to changes in runoff would remain almost the same.

Table 8 lists the mean values of the contribution levels of P and PET after implementing 16 GCMs, along with the changes in mean values of P and PET for the Namhan River Upstream watershed (#1001) and the Dalcheon watershed (#1004). During the NF period of the SSP2–4.5 scenario, the ε_P in the Dalcheon watershed (#1004) was 1.92, higher than that of the Namhan River Upstream watershed (#1001), which was 1.60 (Table 7). Based on this, it was expected that the contribution of P would be greater for the Dalcheon watershed (#1004) compared to the Namhan River Upstream watershed (#1001). However, the contribution of P was 69.91 % in the Dalcheon watershed (#1004) and 77.70 % in the Namhan River Upstream watershed (#1001), indicating larger contribution in the Namhan River Upstream watershed (#1001). While ε_P for the Dalcheon watershed (#1004) was higher, the ratio of change in P ($\frac{\Delta P}{P}$) was smaller than in the Namhan River Upstream watershed (#1001). As shown in Table 8, during the NF period under the SSP2–4.5 scenario, $\frac{\Delta P}{P}$ in the Dalcheon watershed (#1004) was 0.11, which was smaller than the Namhan River Upstream watershed (#1001) with 0.16. Therefore, despite the larger ε_P, $\Delta Q_P(\varepsilon_P \times \frac{\Delta P}{P})$ can be smaller, leading to a lower λ_P. This implies that the contribution of a climate factor to runoff change (λ) is influenced by not only its sensitivity (ε) but also the ratio of change in P ($\frac{\Delta P}{P}$). Similarly, during the FF period under the SSP2–4.5 scenario and the NF and FF periods under the SSP5–8.5 scenario, the Dalcheon watershed (#1004) exhibited higher ε_P than the Namhan River Upstream watershed (#1001) but lower λ_P. During the FF period under the SSP5–8.5 scenario, the elasticity coefficient of PET for the Dalcheon watershed (#1004) was −0.89, while that of the Namhan River Upstream watershed (#1001) was −0.59. However, the contribution of PET was 19.52 % for the Dalcheon watershed (#1004) and 19.86 % for the Namhan River Upstream watershed (#1001), again indicating its higher contribution level for the Namhan River Upstream watershed (#1001). Consequently, if the magnitude of change in climate factors is relatively low, their impacts on runoff can be smaller than

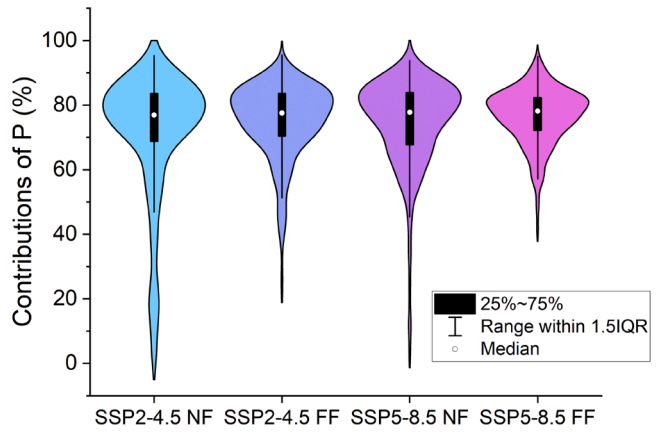

(a)

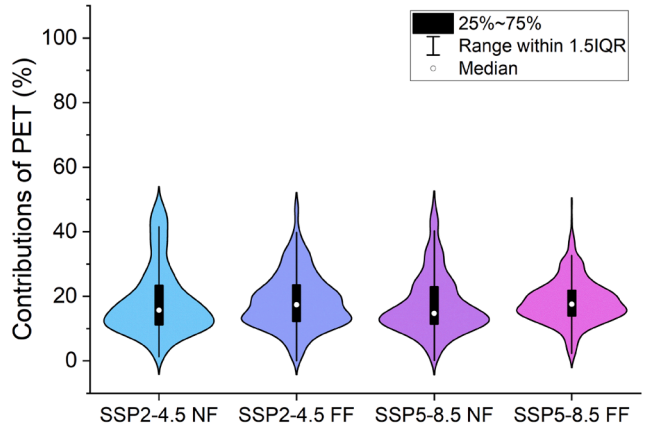

(b)

Fig. 9. (a) Relative contributions of P under different scenarios. (b) The same as (a) but for PET.

those with a higher magnitude of change. However, they can have higher absolute elasticity coefficients.

5. Conclusions

Changes in hydrometeorological variables due to climate change lead to changes in runoff, which can hinder effective water resource management and increase the likelihood of economic, social, and environmental damage. This study simulated changes in future runoff for the Han River basin of South Korea using the GR4J under SSP2–4.5 and SSP5–8.5 scenarios. Furthermore, the climate elasticity method, based on the Budyko framework, was applied to quantify the contributions of P and PET to changes in runoff. This study provides insights into the impacts of climate change on hydrological systems by using projection data from 16 GCMs of CMIP6 under the SSP2–4.5 and SSP5–8.5 scenarios, potentially contributing to water resource management for the anticipated hydrological conditions. The key findings of this study are as follows:

1) Compared to the baseline period (BP: 1975–2020), runoff, P, and PET were projected to increase in the NF (2021–2060) and FF (2061–2100). The magnitudes in the increases were expected to be higher as the periods were farther from the BP.
2) The PET/P is expected to decrease gradually in the future, implying that the climate in the Han River basin may become more humid. The decreasing PET/P also implies that the water cycle will intensify in the Han River basin due to increases in P and temperature.
3) The contribution of P to runoff changes ranged between 67 % and 84 %, while the contribution of PET ranged between 11 % and 24 %. This indicates that P is the primary factor influencing runoff changes in the Han River basin and that the impact of P changes on hydrological conditions is more dominant than that of PET.
4) The elasticity coefficients of P and PET remained consistent throughout the future periods, implying that the long-term impacts of climate change on hydrological systems may not be significantly different from contemporary conditions.
5) Although a high absolute value of the climate elasticity coefficient indicates a higher sensitivity of runoff to a climatic factor, its contribution to runoff can be smaller than that of another case of climate factor if the ratio of change in the climatic factor (e.g., $\frac{\Delta P}{\overline{P}}$ of $\frac{\Delta PET}{\overline{PET}}$) is smaller.

These findings imply that annual runoff variability in the Han River basin is primarily governed by the change in P rather than PET. Climate elasticity coefficient analysis elaborated that P was a dominant factor of runoff variability across sub-basins in different scenarios, underscoring the importance of assessing uncertainties associated with P when evaluating water resources under future climate change scenarios.

This study adopted various GCM datasets to analyze future changes in runoff, P, and PET for the Han River basin. It examined the contribution levels of P and PET to changes in runoff. This study differs from previous research that relied on historical observations or used climate variables without understanding their roles, since we utilized climate change scenario data and quantified the levels of impact of P and PET. Thus, this study can extend the applicability of the Budyko framework and facilitate a clear understanding of the complex effects of climate change on runoff variability, providing a scientific basis for water resource management strategies for domestic, agricultural, and environmental water demands. Meanwhile, using a single hydrological model (i.e., the GR4J) to simulate future runoff may be a limitation of the study due to ignoring model uncertainty. However, since we mainly

Table 8
Contributions and variations of climate factors in the Namhan River Upstream watershed (#1001) and Dalcheon watershed (#1004).

Scenarios	Period	#1001		#1004		#1001		#1004	
		λ_P	λ_{PET}	λ_P	λ_{PET}	$\frac{\Delta P}{\overline{P}}$	$\frac{\Delta PET}{\overline{PET}}$	$\frac{\Delta P}{\overline{P}}$	$\frac{\Delta PET}{\overline{PET}}$
SSP2–4.5	NF	77.70	16.37	69.91	19.25	0.16	0.08	0.11	0.06
	FF	78.04	17.79	71.22	20.33	0.22	0.13	0.18	0.09
SSP5–8.5	NF	80.79	15.13	73.56	18.56	0.19	0.09	0.14	0.07
	FF	76.88	19.86	73.56	19.52	0.29	0.20	0.24	0.13

Units: λ_P, λ_{PET}(%); ΔP, ΔPET(mm).

focus on the implications of multiple GCMs under different climate change scenarios on runoff, a single hydrological model may allow one to pay attention to the role of climate change. For comprehensive analyses, future studies may need to incorporate and compare multiple hydrological models to enable more reliable and accurate projections of future hydrological responses. Furthermore, this study accounted for future uncertainties using data from 16 GCMs of CMIP6 under the SSP2–4.5 and SSP5–8.5 scenarios and showed significant inter-model variability. This variability reflects the uncertainty in future climate projections, directly influencing the magnitude of simulated runoff. Therefore, such uncertainty must be carefully considered when planning and implementing water resource management strategies. While ensemble methods cannot eliminate the inherent uncertainties among individual models, they can reduce the influence of outliers and robustly capture the central tendency. This study provides consistent and interpretable results, which are crucial for practical applications. In addition, future studies should consider not only climatic drivers but also influential anthropogenic factors, such as dam operation and human water usage, to enable more realistic and robust projections of future runoff changes.

CRediT authorship contribution statement

Da Hee Hong: Writing – original draft, Formal analysis, Data curation. **Jeongwoo Han:** Writing – original draft, Methodology, Investigation. **Hyun-Han Kwon:** Visualization, Validation. **Tae-Woong Kim:** Writing – review & editing, Supervision, Funding acquisition.

Declaration of competing interests

The authors declare that they have no known competing financial interests or personal relationships that could have appeared to influence the work reported in this paper.

Acknowledgements

This research was supported by a grant(2022-MOIS63-001, RS-2022-ND641011) of the Cooperative Research Method and Safety Management Technology in National Disaster funded by the Ministry of Interior and Safety (MOIS, Korea).

Supplementary materials

Supplementary material associated with this article can be found, in the online version, at doi:10.1016/j.kscej.2025.100460.

References

Ahn, K. H., & Kim, Y. O. (2019). Incorporating climate model similarities and hydrologic error models to quantify climate change impacts on future riverine flood risk. *Journal of Hydrology, 570*, 118–131. https://doi.org/10.1016/j.jhydrol.2018.12.061

Akhtar, F., Borgemeister, C., Tischbein, B., & Awan, U. K. (2022). Metrics assessment and streamflow modeling under changing climate in a data-scarce heterogeneous region: A case study of the Kabul River Basin. *Water, 14*(11), 1697. https://doi.org/10.3390/w14111697

Anshuman, A., Kunnath-Poovakka, A., & Eldho, T. I. (2021). Performance evaluation of conceptual rainfall-runoff models GR4J and AWBM. *ISH Journal of Hydraulic Engineering, 27*(4), 365–374. https://doi.org/10.1080/09715010.2018.1556124

Badika, P., Raghuvanshi, A. S., & Agarwal, A. (2024). Climate change impact assessment on the hydrological response of the Tawa Basin for sustainable water management. *Groundwater for Sustainable Development.* , Article 101249. https://doi.org/10.1016/j.gsd.2024.101249

Barbhuiya, S., Manekar, A., & Ramadas, M. (2024). Performance evaluation of ML techniques in hydrologic studies: Comparing streamflow simulated by SWAT, GR4J, and state-of-the-art ML-based models. *Journal of Earth System Science, 133*(3), 136. https://doi.org/10.1007/s12040-024-02340-0

Birhanu, D., Kim, H., Jang, C., & Park, S. (2018). Does the complexity of evapotranspiration and hydrological models enhance robustness? *Sustainability, 10*(8), 2837. https://doi.org/10.3390/su10082837

Budyko, M. I. (1974). In D H Miller (Ed.), *Climate and life.* New York, USA: Academic Press.

Chen, H. Y., Huang, C. C., & Yeh, H. F. (2021). Quantifying the relative contribution of climate change and human activity on runoff in the Choshui River Alluvial Fan, Taiwan. *Land, 10*(8), 825. https://doi.org/10.3390/land10080825

Cho, J., Cho, W., & Jung, I. (2018). RSQM: Statistical downscaling toolkit for climate change scenario using nonparametric quantile mapping. http://www.cran.r-project.org/web/packages/rSQM/index.html/ Accessed 22 July 2020.

Collignan, J., Polcher, J., Bastin, S., & Quintana-Segui, P. (2023). Budyko framework-based analysis of the effect of climate change on watershed evaporation efficiency and its impact on discharge over Europe. *Water Resources Research, 59*(10), Article E2023WR034509. https://doi.org/10.1029/2023WR034509

Daly, C., Neilson, R. P., & Phillips, D. L. (1994). A statistical-topographic model for mapping climatological precipitation over mountainous terrain. *Journal of Applied Meteorology and Climatology, 33*(2), 140–158. https://doi.org/10.1175/1520-0450(1994)033≤0140:ASTMFM≥2.0.CO;2

Darbandsari, P., & Coulibaly, P. (2020). Inter-comparison of lumped hydrological models in data-scarce watersheds using different precipitation forcing data sets: Case study of Northern Ontario. *Canada. Journal of Hydrology: Regional Studies, 31*, Article 100730. https://doi.org/10.1016/j.ejrh.2020.100730

Demirel, M. C., Booij, M. J., & Hoekstra, A. Y. (2013). Effect of different uncertainty sources on the skill of 10-day ensemble low-flow forecasts for two hydrological models. *Water Resources Research, 49*(7), 4035–4053. https://doi.org/10.1002/wrcr.20294

Doi, M. V., & Kim, J. (2022). Future projections and uncertainties of CMIP6 for hydrological indicators and their discrepancies from CMIP5 over South Korea. *Water, 14*(18), 2926. https://doi.org/10.3390/w14182926

Ekolu, J., Dieppois, B., Diop, S. B., Bodian, A., Grimaldi, S., Salamon, P., & Tramblay, Y. (2025). How could climate change affect the magnitude, duration and frequency of hydrological droughts and floods in West Africa during the 21st century? A storyline approach. *Journal of Hydrology.* , Article 133482. https://doi.org/10.1016/j.jhydrol.2025.133482

Flynn, C. M., & Mauritsen, T. (2020). On the climate sensitivity and historical warming evolution in recent coupled model ensembles. *Atmospheric Chemistry and Physics, 20*(13), 7829–7842.

Gidden, M. J., Riahi, K., Smith, S. J., Fujimori, S., Luderer, G., Kriegler, E., et al. (2019). Global emissions pathways under different socioeconomic scenarios for use in CMIP6: A dataset of harmonized emissions trajectories through the end of the century. *Geoscientific Model Development, 12*(4), 1443–1475. https://doi.org/10.5194/gmd-12-1443-2019

Gu, L., Yin, J., Wang, S., Chen, J., Qin, H., Yan, X., He, S., & Zhao, T. (2023). How well do the multi-satellite and atmospheric reanalysis products perform in hydrological modelling. *Journal of Hydrology, 617*, Article 128920. https://doi.org/10.1016/j.jhydrol.2022.128920

Gupta, H. V., Kling, H., Yilmaz, K. K., & Martinez, G. F. (2009). Decomposition of the mean squared error and NSE performance criteria: Implications for improving hydrological modelling. *Journal of Hydrology, 377*(1–2), 80–91. https://doi.org/10.1016/j.jhydrol.2009.08.003

Hur, J., Jo, J. P., Jo, S., Shim, K. M., Kim, Y. S., Kang, M. G., & Kim, E. S. (2024). SSP climate change scenarios with 1km resolution over Korean peninsula for agricultural uses. *Korean Journal of Agricultural and Forest Meteorology, 26*(1), 1–30. https://doi.org/10.5532/KJAFM.2024.26.1.1 (in Korean with English abstract).

IPCC. (2021). Climate Change 2021: The physical science basis. *Contribution of working group i to the sixth assessment report of the intergovernmental panel on climate change.* Cambridge, United Kingdom and New York, NY, USA: Cambridge University Press. https://doi.org/10.1017/9781009157896. Masson-Delmotte, V., P. Zhai, A. Pirani, S.L. Connors, C. Péan, S. Berger, N. Caud, Y. Chen, L. Goldfarb, M.I. Gomis, M. Huang, K. Leitzell, E. Lonnoy, J.B.R. Matthews, T.K. Maycock, T. Waterfield, O. Yelekçi, R. Yu, and B. Zhou.

IPCC. (2023). Climate Change 2023: Synthesis Report, summary for policymakers. In H. Lee, & J. Romero (Eds.), *Contribution of working groups i, ii and iii to the sixth assessment report of the intergovernmental panel on climate change.* Geneva, Switzerland: IPCC.

Kim, S., Kim, H., Kim, K., Jun, S. M., Hwang, S., & Kang, M. S. (2021). Assessing the hydroclimatic movement under future scenarios including both climate and land use changes. *Water, 13*(8), 1120. https://doi.org/10.3390/w13081120

Knoben, W. J., Freer, J. E., & Woods, R. A. (2019). Inherent benchmark or not? Comparing Nash–Sutcliffe and Kling–Gupta efficiency scores. *Hydrology and Earth System Sciences, 23*(10), 4323–4331. https://doi.org/10.5194/hess-23-4323-2019

Krajewski, A., Sikorska-Senoner, A. E., Hejduk, L., & Banasik, K. (2021). An attempt to decompose the impact of land use and climate change on annual runoff in a small agricultural catchment. *Water Resources Management, 35*(3), 881–896. https://doi.org/10.1007/s11269-020-02752-9

Lujano, A., Sanchez-Delgado, M., & Lujano, E. (2023). Improvement of Hargreaves–Samani reference evapotranspiration estimates in the Peruvian Altiplano. *Water, 15*(7), 1410. https://doi.org/10.3390/w15071410

Ma, Y., Sun, D., Niu, Z., & Wang, X. (2023). Contribution of climate change and human activities to runoff and sediment discharge changes based on Budyko theory and water-sediment relationships during 1960–2019 in the Taohe River Basin, China. *Atmosphere, 14*(7), 1144. https://doi.org/10.3390/atmos14071144

Malede, D. A., Elumalai, V., Andualem, T. G., Mekonnen, Y. G., Yibeltal, M., Demeke, G. G., & Ray, R. L. (2025). Understanding flood and drought extremes under a changing climate in the Blue Nile Basin: A review. *Environmental and Sustainability Indicators.* , Article 100638. https://doi.org/10.1016/j.indic.2025.100638

Meresa, H., Donegan, S., Golian, S., & Murphy, C. (2022). Simulated changes in seasonal and low flows with climate change for Irish catchments. *Water, 14*(10), 1556. https://doi.org/10.3390/w14101556

Moriasi, D. N., Arnold, J. G., Van Liew M, W., Bingner, R. L., Harmel, R. D., & Veith, T. L. (2007). Model evaluation guidelines for systematic quantification of accuracy in watershed simulations. *Transactions of the ASABE, 50*(3), 885–900. https://doi.org/10.3390/w14101556

Munajat, C. M. (2020). The improvement of Gr4j modeling parameter to estimate unit hydrograph. In *HATHI 6th International Seminar on Advancement of Water Resources Management in a Global Challenge* (p. 6).

Nash, J. E., & Sutcliffe, J. V. (1970). River flow forecasting through conceptual models part I—A discussion of principles. *Journal of Hydrology, 10*(3), 282–290. https://doi.org/10.1016/0022-1694(70)90255-6

Nigatu, Z. M., Fan, D., You, W., & Melesse, A. M. (2021). Hydroclimatic extremes evaluation using GRACE/GRACE-FO and multidecadal climatic variables over the Nile river basin. *Remote Sensing, 13*(4), 651. https://doi.org/10.3390/rs13040651

Noh, S. J., Lee, G., Kim, B., Lee, S., Jo, J., & Woo, D. K. (2024). Climate change impact assessment on water resources management using a combined multi-model approach in South Korea. *Journal of Hydrology: Regional Studies, 53*, Article 101842. https://doi.org/10.1016/j.ejrh.2024.101842

O'Neill, B. C., Tebaldi, C., Van Vuuren D, P., Eyring, V., Friedlingstein, P., Hurtt, G., et al. (2016). The scenario model intercomparison project (ScenarioMIP) for CMIP6. *Geoscientific Model Development, 9*(9), 3461–3482. https://doi.org/10.5194/gmd-9-3461-2016

Oudin, L., Andréassian, V., Perrin, C., Michel, C., & Le Moine, N. (2008). Spatial proximity, physical similarity, regression and ungaged catchments: A comparison of regionalization approaches based on 913 French catchments. *Water Resources Research, 44*(3). https://doi.org/10.1029/2007WR006240

Parajka, J., Merz, R., & Blöschl, G. (2005). A comparison of regionalisation methods for catchment model parameters. *Hydrology and Earth System Sciences, 9*(3), 157–171. https://doi.org/10.5194/hess-9-157-2005

Perrin, C., Michel, C., & Andréassian, V. (2003). Improvement of a parsimonious model for streamflow simulation. *Journal of Hydrology, 279*(1–4), 275–289. https://doi.org/10.1016/S0022-1694(03)00225-7

Sankarasubramanian, A., Vogel, R. M., & Limbrunner, J. F. (2001). Climate elasticity of streamflow in the United States. *Water Resources Research, 37*(6), 1771–1781. https://doi.org/10.1029/2000WR900330

Santos, L., Thirel, G., & Perrin, C. (2018). Pitfalls in using log-transformed flows within the KGE criterion. *Hydrology and Earth System Sciences, 22*(8), 4583–4591. https://doi.org/10.5194/hess-22-4583-2018

Schaake, J. C. (1990). From climate to flow. In J. Smith (Ed.), *Water resour. res.* New York, USA: Wiley.

Séne, S. M. K., Faye, C., & Pande, C. B. (2024). Assessment of current and future trends in water resources in the Gambia River Basin in a context of climate change. *Environmental Sciences Europe, 36*(1), 32. https://doi.org/10.1186/s12302-024-00848-2

Shin, M. J., & Jung, Y. (2022). Using a global sensitivity analysis to estimate the appropriate length of calibration period in the presence of high hydrological model uncertainty. *Journal of Hydrology, 607*, Article 127546. https://doi.org/10.1016/j.jhydrol.2022.127546

Siabi, E. K., Awafo, E. A., Kabo-bah, A. T., Derkyi, N. S. A., Akpoti, K., Mortey, E. M., & Yazdanie, M. (2023). Assessment of Shared Socioeconomic Pathway (SSP) climate scenarios and its impacts on the Greater Accra region. *Urban Climate, 49*, Article 101432. https://doi.org/10.1016/j.uclim.2023.101432

Sinha, J., Sharma, A., Khan, M., & Goyal, M. K. (2018). Assessment of the impacts of climatic variability and anthropogenic stress on hydrologic resilience to warming shifts in Peninsular India. *Scientific Reports, 8*(1), Article 13833. https://doi.org/10.1038/s41598-018-32091-0

Song, Y. H., Chung, E. S., & Shahid, S. (2022). Uncertainties in evapotranspiration projections associated with estimation methods and CMIP6 GCMs for South Korea. *The Science of the Total Environment, 825*, Article 153953. https://doi.org/10.1016/j.scitotenv.2022.153953

Song, Y. H., Chung, E. S., Shahid, S., Kim, Y., & Kim, D. (2023). Development of global monthly dataset of CMIP6 climate variables for estimating evapotranspiration. *Scientific Data, 10*(1), 568. https://doi.org/10.1038/s41597-023-02475-7

Swain, S. S., Kumar, S. B., Mishra, A., & Chatterjee, C. (2023). Sensitive or resilient catchment?: A Budyko-based modeling approach for climate change and anthropogenic stress under historical to CMIP6 future scenarios. *Journal of Hydrology, 622*, Article 129651. https://doi.org/10.1016/j.jhydrol.2023.129651

Themeßl, M. J., Gobiet, A., & Leuprecht, A. (2011). Empirical-statistical downscaling and error correction of daily precipitation from regional climate models. *International Journal of Climatology, 31*(10), 1530–1544. https://doi.org/10.1002/joc.2168

Trenberth, K. E. (2005). The impact of climate change and variability on heavy precipitation, floods, and droughts. *Encyclopedia of Hydrological Sciences, 17*, 1–11.

Vo, T. Q., Van Doi, M., & Kim, J. (2024). Assessment of future changes in drought characteristics through stochastic downscaling and CMIP6 over South Korea. *Stochastic Environmental Research and Risk Assessment*, 1–25. https://doi.org/10.1007/s00477-024-02664-9

Wang, J., Wang, G., Elmahdi, A., Bao, Z., Yang, Q., Shu, Z., & Song, M. (2021). Comparison of hydrological model ensemble forecasting based on multiple members and ensemble methods. *Open Geosciences, 13*(1), 401–415. https://doi.org/10.1515/geo-2020-0239

Xing, W., Wang, W., Zou, S., & Deng, C. (2018). Projection of future runoff change using climate elasticity method derived from Budyko framework in major basins across China. *Global and Planetary Change, 162*, 120–135. https://doi.org/10.1016/j.gloplacha.2018.01.006

Xiong, M., Huang, C. S., & Yang, T. (2020). Assessing the impacts of climate change and land use/cover change on runoff based on improved Budyko framework models considering arbitrary partition of the impacts. *Water, 12*(6), 1612. https://doi.org/10.3390/w12061612

Zelinka, M. D., Myers, T. A., McCoy, D. T., Po-Chedley, S., Caldwell, P. M., Ceppi, P., & Taylor, K. E. (2020). Causes of higher climate sensitivity in CMIP6 models. *Geophysical Research Letters, 47*(1), Article E2019GL085782. https://doi.org/10.1029/2019GL085782

Zhang, L., Dawes, W. R., & Walker, G. R. (2001). Response of mean annual evapotranspiration to vegetation changes at catchment scale. *Water Resources Research, 37*(3), 701–708. https://doi.org/10.1029/2000WR900325

Zheng, J., He, Y., Jiang, X., Nie, T., & Lei, Y. (2021). Attribution analysis of runoff variation in Kuye River Basin based on three Budyko methods. *Land, 10*(10), 1061. https://doi.org/10.3390/land10101061